Nanoscale

PAPER

View Article Online
View Journal | View Issue

Cite this: *Nanoscale*, 2022, **14**, 410

Improved *zT* in Nb_5Ge_3–GeTe thermoelectric nanocomposite†

Jing Cao, [a] Xian Yi Tan, [a,b] Ning Jia,[b] Da Lan,[c] Samantha Faye Duran Solco, [a] Kewei Chen,[d] Sheau Wei Chien,[a] Hongfei Liu,[a] Chee Kiang Ivan Tan,[a] Qiang Zhu, [a] Jianwei Xu,[a] Qingyu Yan [b] and Ady Suwardi *[a,c]

Robust electronic transport properties is a crucial in designing high performance thermoelectrics. A key similarity between superconductor and thermoelectric lies in their generally high electrical conductivity, even at above its superconducting temperature. In this work, we design a nanocomposite between Nb_5Ge_3 and GeTe-based thermoelectric to improve its thermoelectric figure of merit *zT*. Phase and microstructural characterization shows distinct Nb_5Ge_3 precipitates embed in $Ge_{0.9}Sb_{0.1}Te$ matrix. In addition, experimental electronic and thermal transport analysis, together with density functional theory calculation were employed to show the synergistic effect of doping Sb and Nb_5Ge_3 nanocomposite approach. 10% Sb doping was found to optimize the electronic properties of the GeTe-based matrix. Further addition of 2 wt% Nb_5Ge_3 nanocomposite to the matrix enhances the phonon scattering, which consequently lowers the lattice thermal conductivity, which results in *zT* of up to 2.0 at 723 K. Such superconductor nanocomposite approach shown in this work can be employed to enhance the properties of other thermoelectric materials.

Received 21st October 2021,
Accepted 15th December 2021

DOI: 10.1039/d1nr06962d

rsc.li/nanoscale

Introduction

In order to disentangle rapid technological progresses from excessive carbon emission, energy efficiency and recovery is crucial. Amongst many green energy initiatives such as solar cells and wind energy, waste heat harvesting is an area that is often overlooked.[1–5] Thermoelectrics, which recycles waste heat to electricity, is a key technology cut out for this purpose. At the materials level, the efficiency of a thermoelectrics depends on $zT = S^2\sigma T/\kappa$, with S, σ, and κ denoting Seebeck coefficient, electrical, and thermal conductivity, respectively. Intuitively, a good thermoelectric material should have high Seebeck coefficient and electrical conductivity, with low thermal conductivity. This will enable it to maintain robust temperature gradient while generating enough useful power. However, these properties have negative interdependencies on each other, making it an optimization problem. For instance, S and σ are interrelated through n, carrier concentration *via*:

$$S = \frac{8\pi^2 {\kappa_B}^2 T}{3eh^2} m_s^* \left(\frac{\pi}{3n}\right)^{2/3} \quad (1)$$

$$\sigma = ne\mu = \frac{ne^2\tau}{m_l^*}. \quad (2)$$

There are a few limited ways to simultaneously enhance S and σ. For instance, by engineering band convergence, a high value of m_s^* (density of states effective mass) relative to m_l^* (inertial effective mass) can be obtained, resulting in enhanced power factor ($S^2\sigma$). Besides band convergence, other strategies to achieve higher performance (zT) such as nanostructuring, magnetic inclusions, tuning scattering parameters, defect engineering, and dynamic doping are widely used.[6–19]

In recent years, germanium telluride (GeTe) has emerged as one of the best medium temperature thermoelectric materials, with power conversion efficiency above 10%.[20–23] This is primarily due to its Peierls distortion, which renders low thermal conductivity, combined with its robust electronic transport properties and its favourable band structure.[24–40] Nevertheless, GeTe suffers from excessive hole concentration. Therefore, most of the efforts on GeTe have focused on counter doping to optimize carrier concentration with higher valence cation (*i.e.* Bi or Sb).[20,41–51] In addition, doping or alloying with Ti, Cr, Bi_2Te_3, PbTe, Cu_2Te, $AgBiSe_2$, and heat treatment have also

[a]*Institute of Materials Research and Engineering, Agency for Science, Technology and Research, #08-03, 2 Fusionopolis Way, Singapore 138634.*
E-mail: ady_suwardi@imre.a-star.edu.sg
[b]*School of Materials Science and Engineering, Nanyang Technological University, Singapore 639798*
[c]*Department of Materials Science and Engineering, National University of Singapore, Singapore 117575*
[d]*School of Mechanical and Aerospace Engineering, Nanyang Technological University, Singapore 639798*

†Electronic supplementary information (ESI) available. See DOI: 10.1039/d1nr06962d

been explored.[41,52–63] In addition, extremely rapid cooling using liquid nitrogen have also been reported to enhance GeTe performance.[64] More recently, resonant states and entropy engineering have also been reported to improve performance.[65–74] However, the temperature at which the peak performance occurs in GeTe typically lies at the range of 600–800 K. This coincides with its rhombohedral to cubic phase transition. Unfortunately, the phase transition usually results in poor mechanical properties.[75–77] In addition, the lattice thermal conductivity is generally higher in cubic phase, therefore limiting the maximum performance of cubic GeTe.

Among the numerous strategies to enhance thermoelectric properties, nanocomposite approach has been well studied in other materials system such as BiSbTe, PbTe, and SnTe.[78–80] However, such approach has rarely been studied in GeTe to date. This is primarily due to overwhelming focus to either optimize its carrier concentration, or tuning its phase transition temperature. In this work, we report the synergistic effect of nanocomposite approach by adding superconductor Nb_5Ge_3 into $Ge_{0.9}Sb_{0.1}Te$ matrix. Different weight percentage of Nb_5Ge_3 was added and their electronic and thermal transport properties were analyzed. For the matrix phase, 10% Sb was added into GeTe to optimize its carrier concentration.[45,81] By analyzing its intrinsic electronic transport quality *via* weighted-mobility, it was evident that due to the high mobility of superconductor even at its normal state, adding Nb_5Ge_3 only slightly deteriorates its weighted-mobility, while greatly reduces its lattice thermal conductivity. This results in overall enhancement in the zT of $Ge_{0.9}Sb_{0.1}Te$ from 1.7 to 2.0 at 723 K. It is noteworthy that due its high electrical conductivity, the addition of Nb_5Ge_3 results in minimal decrease in overall electronic transport properties of the nanocomposite. In addition, it also helps to preserve slight excess in cation (Ge), which has been shown to be effective in optimizing hole concentration in GeTe.[82] This work opens up exciting avenue of pairing superconductor and thermoelectric as nanocomposite to enhance thermoelectric properties.

Methods

Bulk pellets of $Ge_{0.9}Sb_{0.1}Te$ (denoted GST from hereon) were separately prepared by mixing a stoichiometric amount of high-purity elements (>99.99%) followed by sealing at high vacuum of 10^{-5} mbar in quartz ampoules. Samples were subsequently melted at 1173 K and were occasionally shaken to ensure homogeneity, and were kept at this temperature for 12 hours, followed by quenching in ice water. The final ingots were then pulverized using ball milling (SPEX 8000D, USA) machine. The ball milling were done in SPEX steel-jacketed tungsten carbide jar with tungsten carbide balls, sealed in a Ar atmosphere. The resulting fine powder was subsequently consolidated using spark plasma sintering (SPS) at 673 K for 10 minutes under a pressure of 50 MPa. Extra caution was taken during the cooling down by slow cooling at 15 K min^{-1} and slowly releasing the pressure to the die to avoid cracking the sample. The size of the graphite die was 12.7 mm in diameter. The sintering was done at 1 Pa vacuum. The final density of the pellets was tested using Archimedes method (~98% theoretical density). Nb_5Ge_3 was prepared from its raw elemental constituents by ball milling in stainless steel jacketed tungsten carbide jar (SPEX 8000D) and milled for 6 hours. Part of the final powder was consolidated using spark plasma sintering (SPS) at 673 K for 10 minutes for further testing. The rest of the powders were mixed into GeTe powder before SPS. The Hall carrier concentration was measured using ECOPIA HMS-5500 with 0.5 T magnetic field.

Ady Suwardi

Ady Suwardi obtained his Ph.D. in Materials Science from University of Cambridge, UK. He is currently a group leader at the Institute of Materials Research and Engineering (IMRE), and an adjunct faculty in Department of Materials Science and Engineering, National University of Singapore (NUS). His research expertise lies in energy materials, with specific focus on thermoelectric materials. He works on many aspects of thermoelectric materials and devices including machine learning augmented thermoelectrics, 3D-printing thermoelectrics, and electronic waste recycling for thermoelectrics. He also works on thermoelectrics for various applications in wearables, IoT, and aerospace.

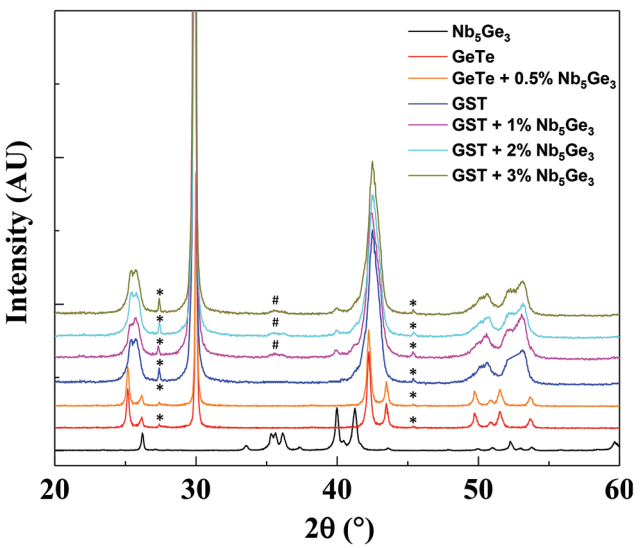

Fig. 1 XRD patterns of pristine GeTe, Nb_5Ge_3, $Ge_{0.9}Sb_{0.1}Te$ (GST), and GST–Nb_5Ge_3 nanocomposites with different wt%. * denotes Ge precipitates peaks, # denotes Nb_5Ge_3 peaks.

The Seebeck coefficient and electrical resistivity were measured using ZEM-3 from ULVAC. Thermal conductivity was measured from LFA 457 Netzsch. The heat capacity used for thermal conductivity calculation was estimated using Dulong–Petit approximation. Microscopy analysis was done in field emission scanning electron microscopy FESEM (JEOL JSM 7600F). TEM was collected using Talos F200X. XRD characterization was conducted using D8 Bruker Advance at room temperature. Magnetic property measurements were performed using Superconducting Quantum Interference Device (SQUID, Quantum Design) in a temperature range of 5 to 50 K. The low temperature electrical resistivity was measured using Quantum Design (QD) PPMS (Physical Properties Measurement System) Evercool II TTO (Thermal Transport Option) module.

Band structure calculations were performed using plane-wave self-consistent code implemented in QUANTUM-ESPRESSO.[83–85] Spin–orbit coupling was taken into consideration during the calculation. The parameterization by Perdew, Burke, and Ernzerhof based on the generalized gradient approximation was used.[86] Atomic coordinates were fully relaxed until the forces on each

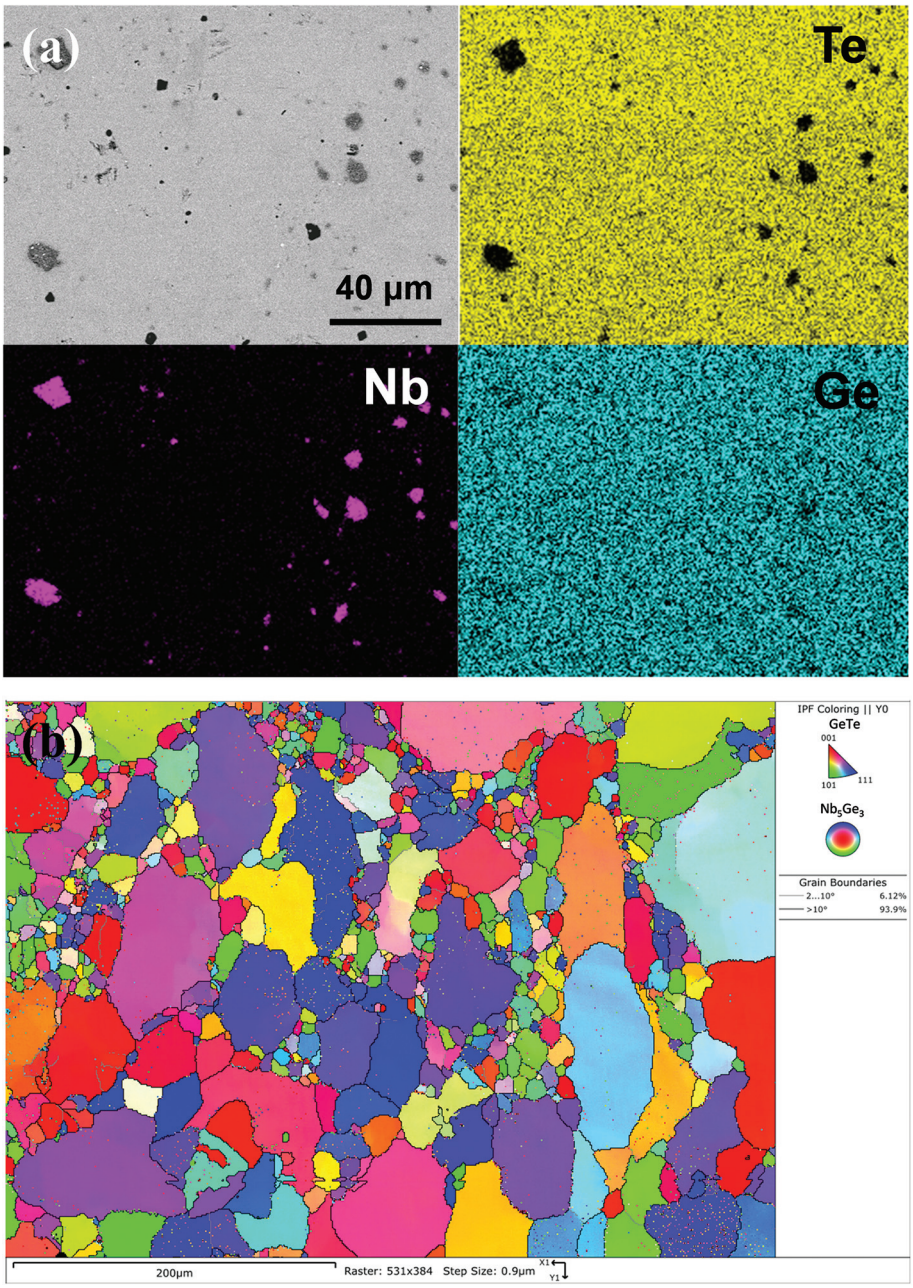

Fig. 2 (a) SEM (scanning electron microscopy) EDS (energy-dispersive X-ray spectroscopy) of the GeTe–Nb_5Ge_3 nanocomposite sample showing Nb-rich regions and Te-poor regions, providing clue of Nb_xGe_y phase in GeTe matrix. (b) EBSD (electron backscatter diffraction) mapping showing large grain sizes, with small Nb_5Ge_3 precipitates within the grains.

atom was less than 10–5 eV $Å^{-1}$. Pristine GeTe in the cubic phase was calculated using the primitive cell. The plane wave cutoff energy was set to 45 Ry. The calculation of GST was based on a 3 × 3 × 3 supercell. The structure was obtained by substituting three Ge atoms with three Sb atom, corresponding to a doping concentration of approximately 11.1%. The plane wave cutoff energy was set to 60 Ry.

Results and discussion

In order to ascertain the phase formation of GST and Nb_5Ge_3, X-ray diffraction (XRD) was done on the final samples, as shown in Fig. 1. It is worth noting that only minute Nb_5Ge_3 peaks can be observed in the GST–Nb_5Ge_3 nanocomposites. This can be attributed to the relatively low volume fraction of Nb_5Ge_3 in GST matrix, considering its much heavier molecular weight (>3 times) compared to GST. In addition, peaks belonging to elemental Ge can be observed at around 28°, consistent with the tendency of GeTe to form Ge precipitates in the matrix.

Further doping of 10% Sb decreases the rhombohedral angle, as evident by the merging of the two peaks around 25°. Importantly, although no Nb_5Ge_3 peak can be observed in the nanocomposite, no shift in peak position or shape can be observed in the three samples with different fraction of Nb_5Ge_3, which can be inferred as no Nb_5Ge_3 goes into the lattice of GST.

To further confirm the presence of Nb_5Ge_3 in GST matrix, SEM EDS was done on the GeTe–Nb_5Ge_3 sample, as shown in Fig. 2 and Fig. S5.† Fig. 2(a) shows the presence of dark regions with sizes <10 μm correspond well to Te-poor and Nb-rich regions, which provides clues of the Nb_xGe_y phase in the GeTe matrix. It is worth noting that no obvious elemental Ge precipitates can be observed in the figure, which is consistent with the reduced Ge-vacancies as will be elaborated in subsequent figures. In addition to elemental mapping, the EBSD (electron backscatter diffraction) mapping in Fig. 2(b) shows large grain size with area-weighted average size of 46 μm (Fig. S1†). In addition, majority of the grains show high-angle boundaries, which has been reported to be effective in reducing thermal conductivity.[87] Furthermore, the presence of Nb_xGe_y is further evident in the uniformly distributed precipitates within each grain.

In order to ascertain that the Nb_xGe_y is indeed Nb_5Ge_3 phase in the precipitates, TEM and HRTEM was carried out, as shown in Fig. 3 and Fig. S6.† Fig. 3(a) shows the elemental mapping in TEM, with zoomed in version of Nb_5Ge_3 phase shown in Fig. 3(b). HRTEM image in Fig. 3(c) shows the (100) and (211) planes of Nb_5Ge_3 phase with lattice spacing

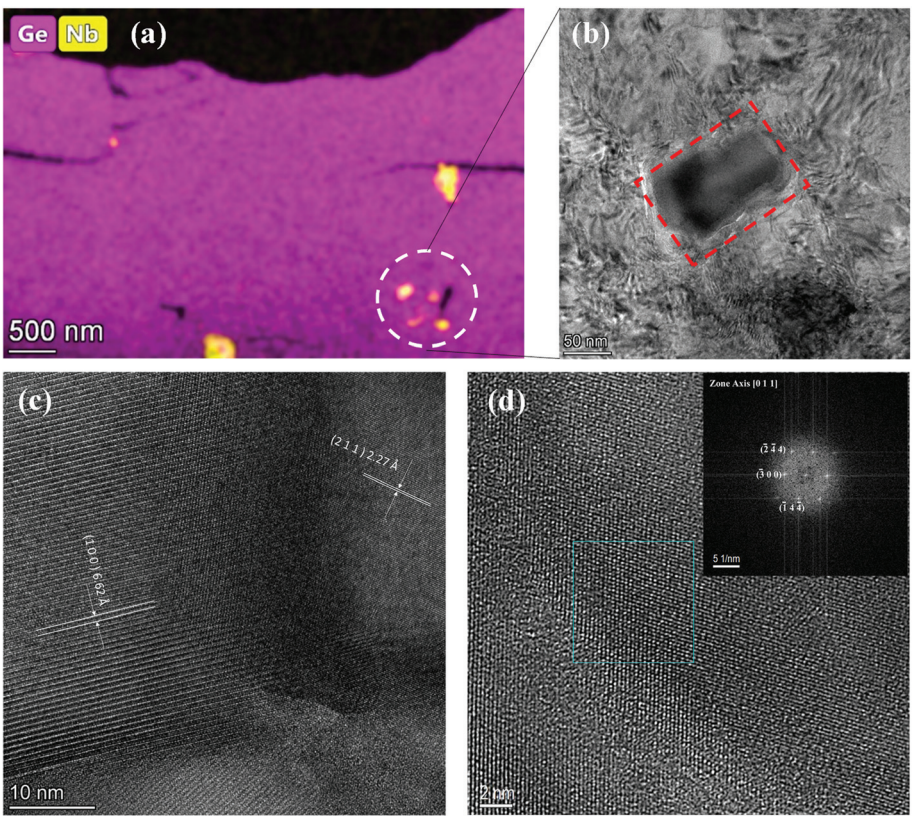

Fig. 3 (a) TEM (transmission electron microscopy) EDS image showing Nb_5Ge_3 phase embed in GeTe matrix. (b) Zoom in image showing Nb_5Ge_3. (c) HRTEM image showing (100) and (211) lattice spacing of Nb_5Ge_3. (d) HRTEM with SAED (selected area electron diffraction) in inset.

of 6.62 Å and 2.27 Å, respectively. The SAED with zone axis (011) is shown in Fig. 3(d), further confirming Nb_5Ge_3 phase signature.

The superconducting properties of Nb_5Ge_3 was characterized using SQUID (superconducting quantum interference device), as shown in Fig. S7.† Temperature dependence of sample magnetization was measured both in zero-field-cooling (ZFC) and field-cooling (FC) processes. In FC process, external magnetic field of 100 Oe was used. The diamagnetic Meissner signal was clear below the temperature ~16 K, indicating the onset of superconducting transition. Magnetic hysteresis loop was measured at 5 K. Since a superconductor is a perfect diamagnet, the sign of magnetic moment is always opposite to that of the external field. Both the Meisnner state and the mixed state can be observed in the loop, exhibiting typical hysteresis loop of type II superconductor. The T_C of 16 K in this work is consistent with previous reports on Nb_5Ge_3 with interstitial carbon doping.[88]

With the Nb_5Ge_3 precipitate phase confirmed by both electron microscopy as well as electronic transport, its effect on thermoelectric properties of GST matrix is subsequently examined, as shown in Fig. 4. Evidently, adding Nb_5Ge_3 into pristine GeTe matrix results in slight increase in Seebeck coefficient, as shown in Fig. 4(a). This is consistent with lower carrier concentration in the sample due to less Ge-vacancies (corresponds to less Ge-precipitates), as confirmed by EDS mapping in Fig. 2 which shows the absence of Ge-precipitates. Further doping of 10% Sb increases the Seebeck coefficient of the samples, with negligible difference between samples with different Nb_5Ge_3 amount.

Fig. 4(b) shows a general trend of increasing resistivity across the entire temperature range with increasing Nb_5Ge_3 wt%, which is also consistent with power factor trend shown in Fig. 4(c). In terms of intrinsic electronic properties, the weighted-mobility, which takes into account the negative interdependencies between Seebeck coefficient and electrical resistivity, is shown in Fig. 4(d). It is evident that while pristine GeTe matrix shows clear acoustic phonon dominated transport, samples with 10% Sb doping show a weaker trend. In addition, introduction of Nb_5Ge_3 only result in small reduction in weighted mobility of all samples, which can be partly attributed to its highly conductive nature. Furthermore, the peaks in weighted mobility at around 650 K can be attributed to rhombohedral–cubic structural phase transition, which results in the convergence of Σ and L band, increasing the overall Seebeck coefficients.

Fig. 5(a) and (b) shows the effect of Sb doping in reducing the hole concentration in GeTe. It is worth noting that the addition of Sb to pristine GeTe results in lowered conduction band, which consequently lead to lowered band gap (from 0.32 eV to 0.15 eV). This is also consistent with the trend of Seeebeck coefficient shown in Fig. 4(a) which shows the downturn of Seebeck coefficients for Sb-doped samples above 723 K. The decrease in Seebeck coefficient at higher temperature can be attributed to thermally activated electron–hole pairs, which results in bipolar conduction, diminishing the net Seebeck coefficient. In contrast, the Seebeck coefficients for pristine GeTe matrix remains in uptrend up to the maximum measure-

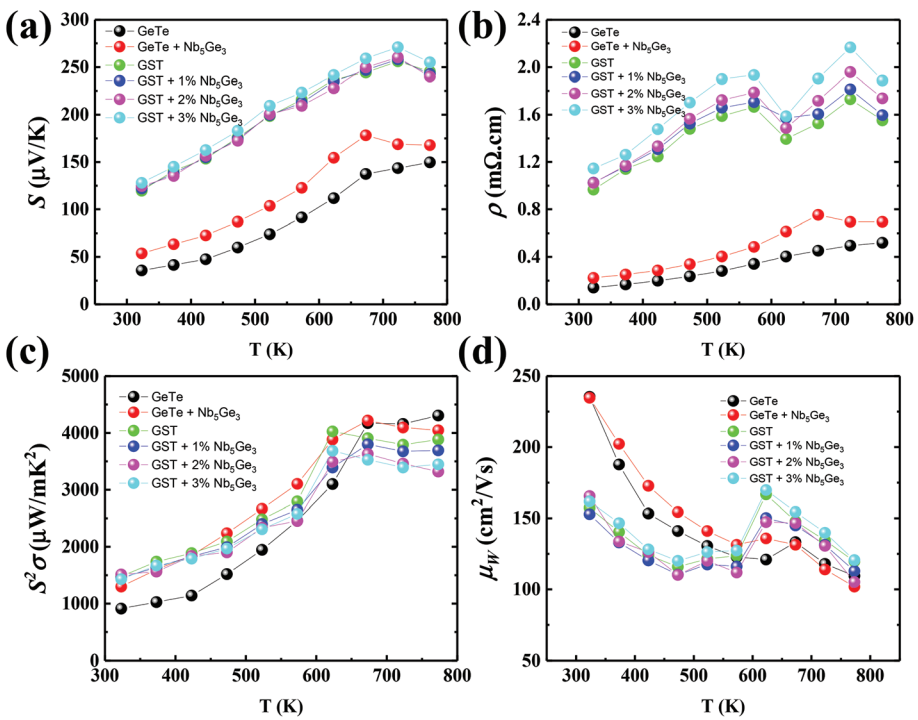

Fig. 4 Temperature dependent (a) Seebeck coefficient (b) electrical resistivity (c) power factor, and (d) weighted-mobility of all samples.

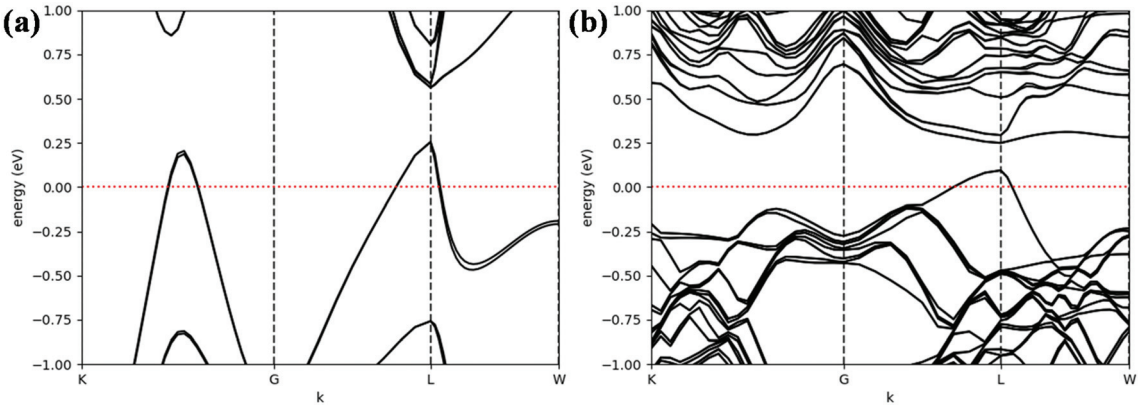

Fig. 5 (a) Electronic band structure of cubic GeTe and (b) cubic $Ge_{0.9}Sb_{0.1}Te$.

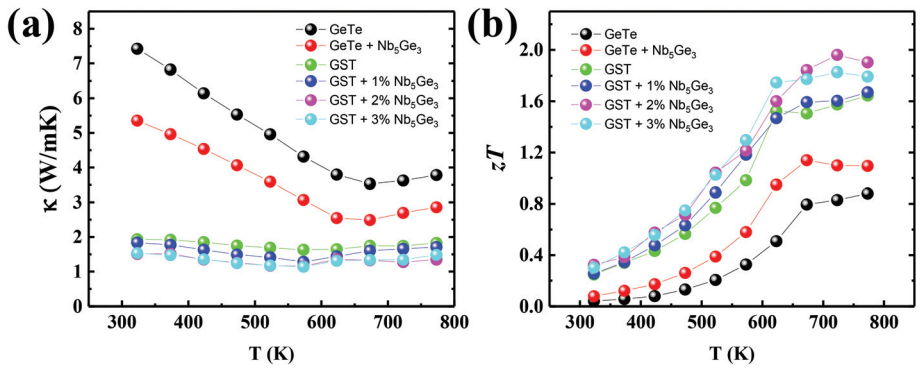

Fig. 6 Temperature dependent (a) total thermal conductivity of all samples. (b) Figure of merit *zT* of all samples.

ment temperature, which can be associated with its higher band gap.

In terms of thermal transport, the addition of Sb and Nb_5Ge_3 greatly reduces the thermal conductivity, as evident in Fig. 6(a), which subsequently result in enhanced *zT* of up to 2.0 at 723 K, as shown in Fig. 6(b). To probe deeper into the origin of the thermal conductivity reduction, it is useful to look into the electronic and lattice contribution to thermal conductivity in all samples. Using Seebeck coefficients data together with electrical resistivity of all samples, the Lorenz number and the electronic contribution to thermal conductivity can be estimated (Fig. S2 and S3†). Furthermore, the lattice thermal conductivity can then be determined by subtracting the electronic thermal conductivity from the total thermal conductivity, as shown in Fig. 7(a). Evidently, the addition of Nb_5Ge_3 systematically reduces the lattice thermal conductivity, which can be used as an independent tuning knob to enhance *zT*.

While it is arguable that addition of Nb_5Ge_3 also decreases the weighted-mobility of the samples, the net effect of which can be examined by plotting it against the lattice thermal conductivity, as illustrated in Fig. 7(b).

In samples with pristine GeTe matrix, the addition of Nb_5Ge_3 results in systematic downshift of lattice thermal conductivity, as shown by the black arrow. In contrast, samples with $Ge_{0.9}Sb_{0.1}Te$ matrix show consistently low lattice thermal conductivity across a range of weighted-mobility, which lends strong support to the role of point defects introduced by Sb dopants in scattering phonons. More importantly, the addition of Nb_5Ge_3 nanocomposite further reduces the lattice thermal conductivity (from green region to blue region) for the same range of weighted-mobility in Nb_5Ge_3–$Ge_{0.9}Sb_{0.1}Te$ nanocomposites.

Finally, the role of grain boundaries, point defects, and nanoprecipitates in reducing lattice thermal conductivity is laid out in Fig. 7(c). It is evident that due to the large grain sizes (46 μm), the grain boundaries play negligible effect in reducing lattice thermal conductivity, consistent with the phonon relaxation time in Fig. S4.† On the other hand, by taking into account point defects due to 10% Sb, the spectral thermal conductivity in Fig. 7(c) is drastically reduced, especially in the high frequency range, resulting in reduced lattice thermal conductivity in Fig. 7(d) (dotted blue curve). Last but not least, nanoprecipitates of Nb_5Ge_3 further reduces the spectral thermal conductivity throughout a wide frequency range, resulting in further reduced lattice thermal conductivity (dotted red curve in Fig. 7(d)).

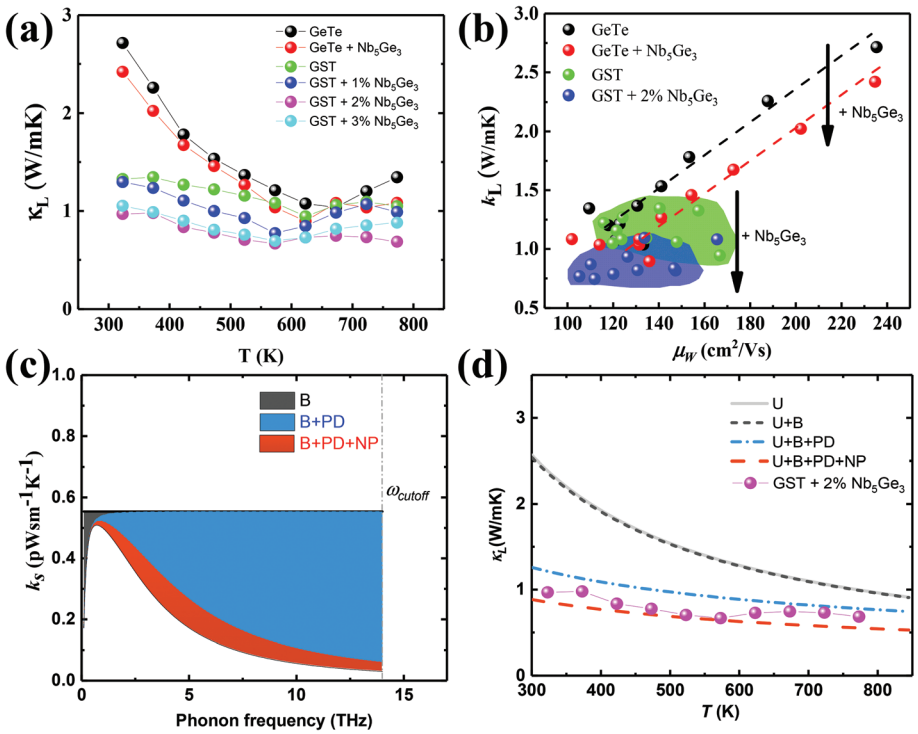

Fig. 7 (a) Temperature dependent lattice thermal conductivity of all samples. (b) Lattice thermal conductivity *vs.* weighted-mobility relation. (c) Spectral thermal conductivity as a function of phonon frequency based on simple Debye–Callaway model taking into account grain boundaries (B), point defects (B + PD), and nanoprecipitates (B + PD + NP) scattering. (d) Modelled lattice thermal conductivity in comparison to experimental values.

Conclusions

In this work, we demonstrate a novel strategy of using nanocomposite approach to enhance zT in thermoelectric matrix. Nb_5Ge_3 precipitates was added to GeTe-based matrix to form the nanocomposites. Further addition of 10% Sb into the GeTe matrix results in optimized doping and hence power factor. Interestingly, Further analysis using simplified Debye–Callaway model and lattice thermal conductivity *versus* weighted-mobility trend clearly demonstrate the benefits of Nb_5Ge_3 in reducing κ_L far outweigh the reduction in weighted-mobility, resulting in enhanced overall zT from 1.7 to 2.0 at 723 K of the nanocomposite. The strategy demonstrated in this work can be used to enhance not only other thermoelectric materials, but also electronic properties of other functional materials in general.

Conflicts of interest

The authors declare no competing financial interest.

Acknowledgements

This work was supported by the A*STAR Computational Resource Centre through the use of its high performance computing facilities. The authors would like to acknowledge Agency for Science, Technology and Research (A*STAR), Singapore Career Development Fund (CDF) C210112022, Sustainable Hybrid Lighting System for Controlled Environment Agriculture programme: A19D9a0096. Q. Yan acknowledges Singapore MOE AcRF Tier 2 under Grant No. 2018-T2-1-010, Singapore A*STAR project A19D9a0096, and the support from FACTS of Nanyang Technological University for sample analysis.

References

1 S. Roychowdhury, T. Ghosh, R. Arora, M. Samanta, L. Xie, N. K. Singh, A. Soni, J. He, U. V. Waghmare and K. Biswas, *Science*, 2021, **371**, 722–727.
2 B. Qin, D. Wang, X. Liu, Y. Qin, J.-F. Dong, J. Luo, J.-W. Li, W. Liu, G. Tan and X. Tang, *Science*, 2021, **373**, 556–561.
3 J. Mao, G. Chen and Z. Ren, *Nat. Mater.*, 2021, **20**, 454–461.
4 F. Qin, S. A. Nikolaev, A. Suwardi, M. Wood, Y. Zhu, X. Tan, U. Aydemir, Y. Ren, Q. Yan, L. Hu and G. J. Snyder, *Chem. Mater.*, 2020, **32**, 10130–10139.
5 X. Wang, A. Suwardi, Y. Zheng, H. Zhou, S. W. Chien and J. Xu, *ACS Appl. Nano Mater.*, 2020, **3**, 10156–10165.
6 X. Qian, H. Wu, D. Wang, Y. Zhang, J. Wang, G. Wang, L. Zheng, S. J. Pennycook and L.-D. Zhao, *Energy Environ. Sci.*, 2019, **12**, 1969–1978.

7 T. Mori, *Small*, 2017, **13**, 1702013.
8 N. Tsujii, A. Nishide, J. Hayakawa and T. Mori, *Sci. Adv.*, 2019, **5**, eaat5935.
9 Y. Xiao and L.-D. Zhao, *Science*, 2020, **367**, 1196–1197.
10 A. Suwardi, L. Hu, X. Wang, X. Y. Tan, D. V. M. Repaka, L.-M. Wong, X. Ni, W. H. Liew, S. H. Lim, Q. Yan, J. Xu, Y. Zheng and K. Hippalgaonkar, *ACS Appl. Mater. Interfaces*, 2020, **12**, 9150–9157.
11 Y. Zheng, T. J. Slade, L. Hu, X. Y. Tan, Y. Luo, Z.-Z. Luo, J. Xu, Q. Yan and M. G. Kanatzidis, *Chem. Soc. Rev.*, 2021, **50**, 9022–9054.
12 N. Jia, J. Cao, X. Y. Tan, J. Dong, H. Liu, C. K. I. Tan, J. Xu, Q. Yan, X. J. Loh and A. Suwardi, *Mater. Today Phys.*, 2021, **21**, 100519.
13 F. Yang, J. Wu, A. Suwardi, Y. Zhao, B. Liang, J. Jiang, J. Xu, D. Chi, K. Hippalgaonkar, J. Lu and Z. Ni, *Adv. Mater.*, 2021, **33**, 2004786.
14 X. Wang, A. Suwardi, S. L. Lim, F. Wei and J. Xu, *npj Flexible Electron.*, 2020, **4**, 19.
15 L. Hu, Y. Luo, Y. W. Fang, F. Qin, X. Cao, H. Xie, J. Liu, J. Dong, A. Sanson and M. Giarola, *Adv. Energy Mater.*, 2021, **11**, 2100661.
16 L. Hu, Y.-W. Fang, F. Qin, X. Cao, X. Zhao, Y. Luo, D. V. M. Repaka, W. Luo, A. Suwardi and T. Soldi, *Nat. Commun.*, 2021, **12**, 1–10.
17 T. Xu, A.-Y. Haruna, Z. Ma, W. Li, J. Li, Y. Luo, D. Zhang and J. Yang, *Chem. Mater.*, 2021, **33**, 8097–8105.
18 Y. Luo, S. Cai, S. Hao, F. Pielnhofer, I. Hadar, Z.-Z. Luo, J. Xu, C. Wolverton, V. P. Dravid and A. Pfitzner, *Joule*, 2020, **4**, 159–175.
19 M. T. Z. Myint, T. Nishikawa, K. Omoto, H. Inoue, Y. Yamashita, A. K. K. Kyaw and Y. Hayashi, *Sci. Rep.*, 2020, **10**, 7307.
20 S. Perumal, M. Samanta, T. Ghosh, U. S. Shenoy, A. K. Bohra, S. Bhattacharya, A. Singh, U. V. Waghmare and K. Biswas, *Joule*, 2019, **3**, 2565–2580.
21 N. Jia, J. Cao, X. Y. Tan, J. Zheng, S. W. Chien, L. Yang, K. Chen, H. K. Ng, S. S. Faye Duran, H. Liu, C. K. Ivan Tan, Z. Li, J. Xu, J. Wu, Q. Yan and A. Suwardi, *J. Mater. Chem. A*, 2021, **9**, 23335–23344.
22 J. Cao, S. W. Chien, X. Y. Tan, C. K. I. Tan, Q. Zhu, J. Wu, X. Wang, Y. Zhao, L. Yang, Q. Yan, H. Liu, J. Xu and A. Suwardi, *ChemNanoMat*, 2021, **7**, 476–482.
23 Z. Liu, N. Sato, W. Gao, K. Yubuta, N. Kawamoto, M. Mitome, K. Kurashima, Y. Owada, K. Nagase and C.-H. Lee, *Joule*, 2021, **5**, 1196–1208.
24 L.-D. Zhao, H. Wu, S. Hao, C.-I. Wu, X. Zhou, K. Biswas, J. He, T. P. Hogan, C. Uher and C. Wolverton, *Energy Environ. Sci.*, 2013, **6**, 3346–3355.
25 A. Banik, U. S. Shenoy, S. Anand, U. V. Waghmare and K. Biswas, *Chem. Mater.*, 2015, **27**, 581–587.
26 L. P. Tan, T. Sun, S. Fan, L. Y. Ng, A. Suwardi, Q. Yan and H. H. Hng, *Nano Energy*, 2013, **2**, 4–11.
27 E. S. Toberer, A. Zevalkink and G. J. Snyder, *J. Mater. Chem.*, 2011, **21**, 15843–15852.
28 A. Banik, T. Ghosh, R. Arora, M. Dutta, J. Pandey, S. Acharya, A. Soni, U. V. Waghmare and K. Biswas, *Energy Environ. Sci.*, 2019, **12**, 589–595.
29 J. Mao, Z. Liu, J. Zhou, H. Zhu, Q. Zhang, G. Chen and Z. Ren, *Adv. Phys.*, 2018, **67**, 69–147.
30 G. J. Snyder and E. S. Toberer, *Materials for sustainable energy: a collection of peer-reviewed research and review articles from Nature Publishing Group*, World Scientific, 2011, pp. 101–110.
31 G. Tan, L.-D. Zhao and M. G. Kanatzidis, *Chem. Rev.*, 2016, **116**, 12123–12149.
32 A. Zevalkink, D. M. Smiadak, J. L. Blackburn, A. J. Ferguson, M. L. Chabinyc, O. Delaire, J. Wang, K. Kovnir, J. Martin and L. T. Schelhas, *Appl. Phys. Rev.*, 2018, **5**, 021303.
33 J. Yang, L. Xi, W. Qiu, L. Wu, X. Shi, L. Chen, J. Yang, W. Zhang, C. Uher and D. J. Singh, *npj Comput. Mater.*, 2016, **2**, 1–17.
34 W. G. Zeier, A. Zevalkink, Z. M. Gibbs, G. Hautier, M. G. Kanatzidis and G. J. Snyder, *Angew. Chem., Int. Ed.*, 2016, **55**, 6826–6841.
35 A. Suwardi, D. Bash, H. K. Ng, J. R. Gomez, D. M. Repaka, P. Kumar and K. Hippalgaonkar, *J. Mater. Chem. A*, 2019, **7**, 23762–23769.
36 E. B. Isaacs and C. Wolverton, *Chem. Mater.*, 2018, **30**, 1540–1546.
37 J. He, Y. Xia, S. S. Naghavi, V. Ozoliņš and C. Wolverton, *Nat. Commun.*, 2019, **10**, 1–8.
38 J. Yan, P. Gorai, B. Ortiz, S. Miller, S. A. Barnett, T. Mason, V. Stevanović and E. S. Toberer, *Energy Environ. Sci.*, 2015, **8**, 983–994.
39 M. Cagnoni, D. Führen and M. Wuttig, *Adv. Mater.*, 2018, **30**, 1801787.
40 R. W. McKinney, P. Gorai, V. Stevanović and E. S. Toberer, *J. Mater. Chem. A*, 2017, **5**, 17302–17311.
41 J. Shuai, X. Tan, Q. Guo, J. Xu, A. Gellé, R. Gautier, J.-F. Halet, F. Failamani, J. Jiang and T. Mori, *Mater. Today Phys.*, 2019, **9**, 100094.
42 L.-D. Zhao, Y. Qiu, Y. Jin, D. Wang, M. Guan, W. He, S. Peng, R. Liu and X. Gao, *J. Mater. Chem. A*, 2019, **7**, 26393–26401.
43 M. Hong, J. Zou and Z. G. Chen, *Adv. Mater.*, 2019, **31**, 1807071.
44 M. Hong, Y. Wang, W. Liu, S. Matsumura, H. Wang, J. Zou and Z. G. Chen, *Adv. Energy Mater.*, 2018, **8**, 1801837.
45 S. Perumal, S. Roychowdhury, D. S. Negi, R. Datta and K. Biswas, *Chem. Mater.*, 2015, **27**, 7171–7178.
46 K. Saheb Bayikadi, S. Raman, C. T. Wu, L.-C. Chen, K. H. Chen and F.-C. Chou, *J. Mater. Chem. A*, 2019, **7**, 15181–15189.
47 B. Srinivasan, C. Boussard-Plédel and B. Bureau, *Mater. Lett.*, 2018, **230**, 191–194.
48 B. Srinivasan, A. Gellé, J.-F. Halet, C. Boussard-Pledel and B. Bureau, *Materials*, 2018, **11**, 2237.
49 B. Srinivasan, S. Le Tonquesse, A. Gellé, C. Bourgès, L. Monier, I. Ohkubo, J.-F. Halet, D. Berthebaud and T. Mori, *J. Mater. Chem. A*, 2020, **8**, 19805–19821.

50 Z. Liu, N. Sato, Q. Guo, W. Gao and T. Mori, *NPG Asia Mater.*, 2020, **12**, 1–11.
51 G. Bai, Y. Yu, X. Wu, J. Li, Y. Xie, L. Hu, F. Liu, M. Wuttig, O. Cojocaru-Mirédin and C. Zhang, *Adv. Energy Mater.*, 2021, **11**, 2102012.
52 Y. Jin, Y. Xiao, D. Wang, Z. Huang, Y. Qiu and L.-D. Zhao, *ACS Appl. Energy Mater.*, 2019, **2**, 7594–7601.
53 K. S. Bayikadi, R. Sankar, C. T. Wu, C. Xia, Y. Chen, L.-C. Chen, K.-H. Chen and F.-C. Chou, *J. Mater. Chem. A*, 2019, **7**, 15181–15189.
54 J. Dong, F.-H. Sun, H. Tang, J. Pei, H.-L. Zhuang, H.-H. Hu, B.-P. Zhang, Y. Pan and J.-F. Li, *Energy Environ. Sci.*, 2019, **12**, 1396–1403.
55 D. Wu, L.-D. Zhao, S. Hao, Q. Jiang, F. Zheng, J. W. Doak, H. Wu, H. Chi, Y. Gelbstein and C. Uher, *J. Am. Chem. Soc.*, 2014, **136**, 11412–11419.
56 Y. Gelbstein, J. Davidow, S. N. Girard, D. Y. Chung and M. Kanatzidis, *Adv. Energy Mater.*, 2013, **3**, 815–820.
57 M. Samanta and K. Biswas, *J. Am. Chem. Soc.*, 2017, **139**, 9382–9391.
58 M. Samanta, T. Ghosh, R. Arora, U. V. Waghmare and K. Biswas, *J. Am. Chem. Soc.*, 2019, **141**, 19505–19512.
59 M. Hong, Y. Wang, T. Feng, Q. Sun, S. Xu, S. Matsumura, S. T. Pantelides, J. Zou and Z.-G. Chen, *J. Am. Chem. Soc.*, 2018, **141**, 1742–1748.
60 E. Nshimyimana, S. Hao, X. Su, C. Zhang, W. Liu, Y. Yan, C. Uher, C. Wolverton, M. G. Kanatzidis and X. Tang, *J. Mater. Chem. A*, 2020, **8**, 1193–1204.
61 J. Shuai, Y. Sun, X. Tan and T. Mori, *Small*, 2020, **16**, 1906921.
62 W. D. Liu, D. Z. Wang, Q. Liu, W. Zhou, Z. Shao and Z. G. Chen, *Adv. Energy Mater.*, 2020, **10**, 2000367.
63 Z. Liu, W. Gao, W. Zhang, N. Sato, Q. Guo and T. Mori, *Adv. Energy Mater.*, 2020, **10**, 2002588.
64 L. Wang, J. Li, C. Zhang, T. Ding, Y. Xie, Y. Li, F. Liu, W. Ao and C. Zhang, *J. Mater. Chem. A*, 2020, **8**, 1660–1667.
65 L. Wu, X. Li, S. Wang, T. Zhang, J. Yang, W. Zhang, L. Chen and J. Yang, *NPG Asia Mater.*, 2017, **9**, e343.
66 Y. Qiu, Y. Jin, D. Wang, M. Guan, W. He, S. Peng, R. Liu, X. Gao and L.-D. Zhao, *J. Mater. Chem. A*, 2019, **7**, 26393–26401.
67 S. Zhi, J. Li, L. Hu, J. Li, N. Li, H. Wu, F. Liu, C. Zhang, W. Ao and H. Xie, *Adv. Sci.*, 2021, 2100220.
68 T. Xing, Q. Song, P. Qiu, Q. Zhang, X. Xia, J. Liao, R. Liu, H. Huang, J. Yang and S. Bai, *Natl. Sci. Rev.*, 2019, **6**, 944–954.
69 Z. Liu, J. Sun, J. Mao, H. Zhu, W. Ren, J. Zhou, Z. Wang, D. J. Singh, J. Sui and C.-W. Chu, *Proc. Natl. Acad. Sci. U. S. A.*, 2018, **115**, 5332–5337.
70 Z. Zheng, X. Su, R. Deng, C. Stoumpos, H. Xie, W. Liu, Y. Yan, S. Hao, C. Uher and C. Wolverton, *J. Am. Chem. Soc.*, 2018, **140**, 2673–2686.
71 A. Suwardi, J. Cao, L. Hu, F. Wei, J. Wu, Y. Zhao, S. H. Lim, L. Yang, X. Y. Tan and S. W. Chien, *J. Mater. Chem. A*, 2020, **8**, 18880–18890.
72 Y. Luo, T. Xu, Z. Ma, D. Zhang, Z. Guo, Q. Jiang, J. Yang, Q. Yan and M. G. Kanatzidis, *J. Am. Chem. Soc.*, 2021, **143**, 13990–13998.
73 Y. Luo, S. Hao, S. Cai, T. J. Slade, Z. Z. Luo, V. P. Dravid, C. Wolverton, Q. Yan and M. G. Kanatzidis, *J. Am. Chem. Soc.*, 2020, **142**, 15187–15198.
74 Z. Ma, T. Xu, W. Li, Y. Cheng, J. Li, D. Zhang, Q. Jiang, Y. Luo and J. Yang, *Adv. Funct. Mater.*, 2021, **31**, 2103197.
75 L. Wang, J. Li, Y. Xie, L. Hu, F. Liu, W. Ao, J. Luo and C. Zhang, *Mater. Today Phys.*, 2021, **16**, 100308.
76 Y. Dou, J. Li, Y. Xie, X. Wu, L. Hu, F. Liu, W. Ao, Y. Liu and C. Zhang, *Mater. Today Phys.*, 2021, **20**, 100497.
77 G. Bai, Y. Yu, X. Wu, J. Li, Y. Xie, L. Hu, F. Liu, M. Wuttig, O. Cojocaru-Mirédin and C. Zhang, *Adv. Energy Mater.*, 2021, 2102012.
78 J. Martin, G. Nolas, W. Zhang and L. Chen, *Appl. Phys. Lett.*, 2007, **90**, 222112.
79 J. He, J. Xu, X. Tan, G.-Q. Liu, H. Shao, Z. Liu, H. Jiang and J. Jiang, *J. Materiomics*, 2016, **2**, 165–171.
80 J. Li, Q. Tan, J. F. Li, D. W. Liu, F. Li, Z. Y. Li, M. Zou and K. Wang, *Adv. Funct. Mater.*, 2013, **23**, 4317–4323.
81 A. Suwardi, S. H. Lim, Y. Zheng, X. Wang, S. W. Chien, X. Y. Tan, Q. Zhu, L. M. N. Wong, J. Cao and W. Wang, *J. Mater. Chem. C*, 2020, **8**, 16940–16948.
82 A. Suwardi, J. Cao, Y. Zhao, J. Wu, S. Chien, X. Tan, L. Hu, X. Wang, W. Wang and D. Li, *Mater. Today Phys.*, 2020, **14**, 100239.
83 P. Giannozzi, S. Baroni, N. Bonini, M. Calandra, R. Car, C. Cavazzoni, D. Ceresoli, G. L. Chiarotti, M. Cococcioni, I. Dabo, A. Dal Corso, S. de Gironcoli, S. Fabris, G. Fratesi, R. Gebauer, U. Gerstmann, C. Gougoussis, A. Kokalj, M. Lazzeri, L. Martin-Samos, N. Marzari, F. Mauri, R. Mazzarello, S. Paolini, A. Pasquarello, L. Paulatto, C. Sbraccia, S. Scandolo, G. Sclauzero, A. P. Seitsonen, A. Smogunov, P. Umari and R. M. Wentzcovitch, *J. Phys.: Condens. Matter*, 2009, **21**, 395502.
84 P. Giannozzi, O. Andreussi, T. Brumme, O. Bunau, M. Buongiorno Nardelli, M. Calandra, R. Car, C. Cavazzoni, D. Ceresoli, M. Cococcioni, N. Colonna, I. Carnimeo, A. Dal Corso, S. de Gironcoli, P. Delugas, R. A. DiStasio, A. Ferretti, A. Floris, G. Fratesi, G. Fugallo, R. Gebauer, U. Gerstmann, F. Giustino, T. Gorni, J. Jia, M. Kawamura, H. Y. Ko, A. Kokalj, E. Küçükbenli, M. Lazzeri, M. Marsili, N. Marzari, F. Mauri, N. L. Nguyen, H. V. Nguyen, A. Otero-de-la-Roza, L. Paulatto, S. Poncé, D. Rocca, R. Sabatini, B. Santra, M. Schlipf, A. P. Seitsonen, A. Smogunov, I. Timrov, T. Thonhauser, P. Umari, N. Vast, X. Wu and S. Baroni, *J. Phys.: Condens. Matter*, 2017, **29**, 465901.
85 P. Giannozzi, O. Baseggio, P. Bonfà, D. Brunato, R. Car, I. Carnimeo, C. Cavazzoni, S. d. Gironcoli, P. Delugas, F. F. Ruffino, A. Ferretti, N. Marzari, I. Timrov, A. Urru and S. Baroni, *J. Chem. Phys.*, 2020, **152**, 154105.
86 J. P. Perdew, K. Burke and M. Ernzerhof, *Phys. Rev. Lett.*, 1996, **77**, 3865–3868.
87 X. Meng, Z. Liu, B. Cui, D. Qin, H. Geng, W. Cai, L. Fu, J. He, Z. Ren and J. Sui, *Adv. Energy Mater.*, 2017, **7**, 1602582.
88 A. D. Bortolozo, C. A. M. d. Santos, R. F. Jardim, C. Ritter, A. Devishvili, M. Rotter, F. G. Gandra and A. J. S. Machado, *J. Appl. Phys.*, 2012, **111**, 123912.

